View metadata, citation and similar papers at core.ac.uk
brought to you by CORE
provided by Kanazawa University Repository for Academic Resources

Thermal-equilibrium defects in undoped hydrogenated amorphous silicon, silicon-carbon, and silicon-nitrogen

著者	Xu Xixiang, Sasaki Hiroyuki, Morimoto Akiharu, Kumeda Minoru, Shimizu Tatsuo
journal or publication title	Physical Review -Series B-
volume	41
number	14
page range	10049-10057
year	1990-05-01
URL	http://hdl.handle.net/2297/24512

doi: 10.1103/PhysRevB.41.10049

Thermal-equilibrium defects in undoped hydrogenated amorphous silicon, silicon-carbon, and silicon-nitrogen

Xixiang Xu,* Hiroyuki Sasaki, Akiharu Morimoto, Minoru Kumeda, and Tatsuo Shimizu
Department of Electronics, Faculty of Technology, Kanazawa University, Kanazawa, Ishikawa 920, Japan
(Received 20 October 1989)

Temperature dependence of the thermal-equilibrium defect density in undoped *a*-Si:H, *a*-$Si_{1-x}C_x$:H, and *a*-$Si_{1-x}N_x$:H is obtained both by *in situ* electron-spin-resonance (ESR) measurements at elevated temperatures and by ESR measurements of frozen-in defects at room temperature. The experimental results confirm that the defects in these alloy films, even for films with the defect density as high as 10^{17} cm^{-3}, can reach thermal equilibrium above a certain temperature (200–350 °C). Thickness dependence of the defect density after various thermal treatments shows that only the bulk defect density increases with temperature, with the exception that thin *a*-Si:H films (<1 μm) exhibit some extra increase. Results of ESR, light-induced ESR (LESR), and constant-photocurrent method (CPM) measurements indicate that the charged-defect density in these films does not appreciably increase with temperature. Relaxation of the frozen-in defect density follows a stretched exponential form and the relaxation time increases with the defect density in these alloys.

I. INTRODUCTION

The density of defects in undoped hydrogenated amorphous silicon (*a*-Si:H) has been found to be able to reach a thermal equilibrium around 200 °C.[1–7] Smith *et al.* first reported the observation of the freeze-in of defects in undoped *a*-Si:H by measuring subband-gap optical absorption by photothermal deflection spectroscopy (PDS) and the constant-photocurrent method (CPM).[2] McMahon and Tsu observed this phenomenon by photoconductivity measurements and found that the thermal-equilibrium temperature T_E was 200±5 °C in undoped *a*-Si:H.[3] By electron-spin-resonance (ESR) measurements, we observed the reversible change with temperature in the density of neutral defects in both *a*-Si:H and *a*-$Si_{1-x}C_x$:H alloy films.[4,5] Recently, Street and Winer observed the frozen-in defects in *a*-Si:H with different defect densities deposited at various deposition conditions by ESR measurements over a wide range of annealing temperature from 180 to 400 °C, and investigated the relaxation behavior of those frozen-in defects.[8] All of these experiments show that the thermal-equilibrium defect density increases with temperature, and the higher defect density above T_E can be frozen in by fast cooling (FC). At the same time, several theoretical models have been proposed to describe the defect reaction and temperature dependence of the thermal-equilibrium defects in *a*-Si:H.[8–13] The formation energy of defects in *a*-Si:H estimated from different models remains to be somewhat controversial, and the values range from 0.13 to 0.57 eV.

The study of thermal-equilibrium defects in *a*-Si:H has also been extended to hydrogenated *a*-Si-based alloy films, such as *a*-$Si_{1-x}C_x$:H (Refs. 4–6) and *a*-$Si_{1-x}Ge_x$:H,[14] which provides important information about the origin of the high defect density in these alloy films. In previous papers,[4–6] we reported that thermal equilibrium can be reached in *a*-$Si_{1-x}C_x$:H with a defect density 2 orders of magnitude higher than that in *a*-Si:H. The effect of thermal equilibration on dark conductivity and photoconductivity in *a*-$Si_{1-x}Ge_x$:F:H alloys was observed by a Princeton group and the freeze-in temperature was reported to be about 140 °C for the alloys with the optical gap of 1.4 eV.[14] In this work, we study the temperature dependence of the thermal-equilibrium defect density and the relaxation behavior of frozen-in defects in *a*-Si:H, *a*-$Si_{1-x}C_x$:H, and *a*-$Si_{1-x}N_x$:H with different alloy contents by means of ESR, light-induced ESR (LESR), CPM, and dark-conductivity measurements. ESR, LESR, and CPM measurements are carried out for the films with various thicknesses in order to know the behavior of both charged defects and surface defects during the equilibrium process.

II. EXPERIMENTAL

a-Si:H, *a*-$Si_{1-x}C_x$:H, and *a*-$Si_{1-x}N_x$:H films used in this study were prepared by an rf glow-discharge (GD) decomposition of SiH_4, SiH_4+CH_4, and SiH_4+NH_3, respectively, with a substrate temperature of 350 °C, and an rf power of 20 W. The films were deposited on fused silica glass substrates for electrical, optical, and ESR measurements. To get a larger amount of specimen for ESR measurements, the films were also deposited on aluminum-foil substrates. The aluminum foil was dissolved in dilute HCl, and the sample flakes were transferred to a quartz sample tube. The thickness of the films was changed from 0.3 to 8 μm.

ESR measurements were performed at *X*-band using a Varian E109 instrument mainly at room temperature, and LESR measurements at 77 K. A xenon lamp with an infrared-cut filter was used as a light source for LESR measurements. The intensity of the light was limited to 3 mW/cm^2 in order to avoid the Staebler-Wronski effect. The absence of the Staebler-Wronski effect was confirmed by comparing the spin density before and after LESR

 ©1990 The American Physical Society

measurements. More details about LESR measurements were reported before.[15]

Coplanar aluminum electrodes were evaporated on the film for conductivity and CPM measurements. During the temperature-dependent conductivity measurements, the rate of the increase in temperature was kept to about 0.015 °C/s. In CPM measurements, the photocurrent was measured with monochromatic light using a 400-W halogen-tungsten lamp. A monochrometer with 10 cm focal length was used, coupled with the interference filter to eliminate a stray light. By fitting the relative optical-absorption coefficient from CPM with the value from optical-absorption measurements, the absorption spectra in the subband-gap absorption region can be obtained. The density of defects related to the subband-gap absorption can be estimated using the fitting method proposed in Ref. 16.

Up to 300 °C, both fast cooling (FC) and slow cooling (SC) were performed after at least 30 min annealing in vacuum (2×10^{-5} Torr). FC was accomplished by dropping the sample into liquid N_2. FC from 400 °C was carried out after only 10 min annealing in atmosphere and then dropping the samples into ice water. The average cooling rate in these methods was estimated to be larger than 10 °C/s. SC was achieved by an automatically controlled cooling system, and its cooling rate was 0.02–0.04 °C/s.

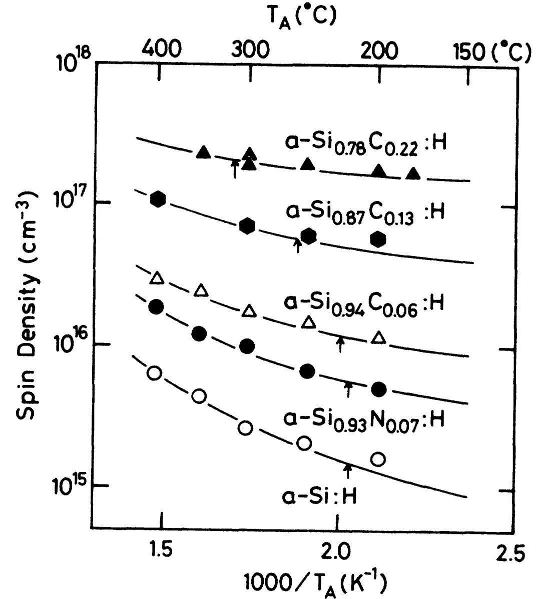

FIG. 1. Dependence of bulk spin densities of the frozen-in defects on annealing temperature T_A for five hydrogenated a-Si-based alloy films. The solid curves are the fitted results with Eq. (2). The arrows indicate the thermal-equilibrium temperature T_E.

III. RESULTS AND DISCUSSION

A. Temperature dependence of defect density

The thermal-equilibrium defect density can be roughly expressed in a thermally activated exponential form,

$$N_D(T)=N_0\exp(-E_f/kT) , \quad (1)$$

where E_f is the formation energy of defects.[8] The defect density is expected to increase with temperature with an activation energy of E_f. Therefore, the temperature dependence of the thermal-equilibrium defect density can be obtained both by a direct *in situ* measurement at elevated temperature by heating samples and a room-temperature measurement after FC of samples from annealing temperature in which thermal-equilibrium defects at the annealing temperature should be frozen in if the cooling rate is high enough.

Temperature dependence of the thermal-equilibrium density of defects in undoped a-Si:H, a-$Si_{1-x}C_x$:H, and a-$Si_{1-x}N_x$:H detected by ESR measurements are shown in Figs. 1 and 2, in which we subtract off the surface defect contribution to the total defect density. In Fig. 1, the spin densities of the frozen-in defects measured at room temperature are plotted against the annealing temperature T_A for five different alloy samples. These spins are attributed to neutral dangling bonds. At each temperature, the samples were first annealed for a time long enough for the defects to reach the thermal equilibration, e.g., a-Si:H being annealed for 1 h at 250 °C, but only 10 min at 400 °C (a short annealing time at high temperature can avoid the irreversible change in the defect density). The spin densities shown in Fig. 1 for all five samples increase remarkably with T_A, indicating that the thermal-equilibrium process can occur in all these undoped hydrogenated amorphous silicon-based alloy films although the spin densities range from 10^{15} to 10^{17} cm^{-3}. A larger relative increase in the defect density appears in the less alloy-content samples. For a-Si:H, FC from 400 °C in-

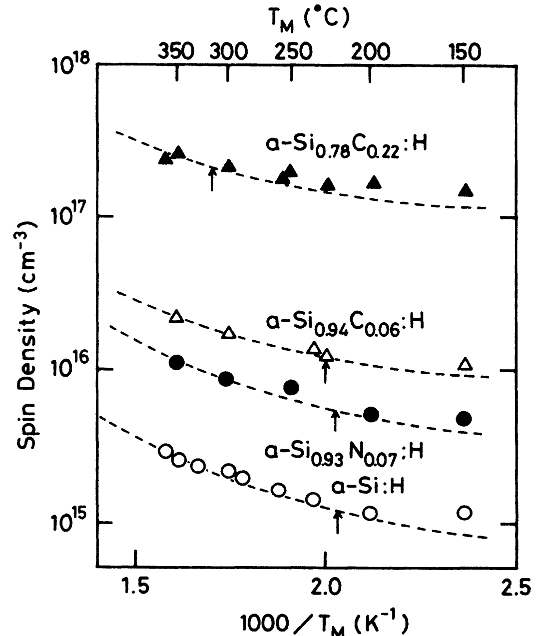

FIG. 2. Dependence of bulk spin densities on measurement temperature T_M for the alloy films. The dashed curves are guides for the eye. The arrows indicate T_E.

creases the spin density by a factor 4, but the same procedure only increases the spin density by a factor 1.8–2.0 for a-$Si_{0.87}C_{0.13}$:H which has a spin density of 10^{17} cm^{-3}. The formation energy of the defect estimated from a high-temperature side (250–400 °C) also decreases with the spin density, and E_f is about 0.2 eV for a-Si:H and 0.14 eV for a-$Si_{0.87}C_{0.13}$:H. The solid curves are the fitted results which will be described below.

In order to check whether or not the FC process itself causes the changes in the defect density, the *in situ* ESR measurements at elevated temperatures were also made by heating the samples up to about 350 °C. Figure 2 shows the measurement-temperature dependence of the spin density of these samples. Both general trends of temperature dependence and magnitudes of the defect density shown in Fig. 2 agree quite well with those in Fig. 1, indicating that the frozen-in defect density measured after FC is the thermal-equilibrium defect density at the annealing temperature.

Here we adopt a new model of Smith and Wagner to fit our experimental data.[10] Smith and Wagner introduced a distribution of formation energies of defects and associated it with the exponential distribution of the valence-band-tail states. By minimizing the free energy of the system, a Boltzmann fraction of valence-band-tail states is able to convert to dangling bonds. The density of dangling bonds $N_D(T)$ is contributed to the following two terms,

$$\begin{aligned} N_D(T) &= \int_0^{E_d} g(E)\exp[-U(E)/kT]dE + \int_{E_d}^{\infty} g(E)dE \\ &= \int_0^{E_d} N_{vt}\exp(-E/E_u)\exp[-(E_d-E)/kT]dE + \int_{E_d}^{\infty} N_{vt}\exp(-E/E_u)dE \\ &= N_{vt}[E_u kT/(E_u-kT)][\exp(-E_d/E_u)-\exp(-E_d/kT)] + N_{vt}E_u\exp(-E_d/E_u) \ , \end{aligned} \quad (2)$$

where E_d is the energy level of the neutral dangling bonds, the origin of the energy being taken at the joint point of the exponential and linear regions of the density of the valence-band-tail state $g(E)$, $N_{vt}=g(0)$, $U=E_d-E$, and E_u is a characteristic energy of Urbach tail. It is noteworthy that the second term in Eq. (2) is independent of temperature. This term was neglected by Smith *et al.* for a-Si:H. When $T=0$, the defect density comes from this term, which is just the number of valence-band-tail states above E_d.

We used this model to fit our experimental results for hydrogenated a-Si-based alloys. It is assumed that in Si-dominated alloys (a-$Si_{1-x}A_x$:H, A=C or N, $X \ll 0.5$), the effect of the addition of alloy elements such as C or N is only the broadening of the valence-band tail and the change in the optical gap. Strictly speaking, details of Si—C or Si—N bonding scheme should be taken in account in the model, but we ignored them here. As shown in Fig. 1, the experimental data for the undoped hydrogenated a-Si-based alloy films were fitted with Eq. (2) with the fitting parameters listed in Table I. The temperature dependence of the defect density can be reproduced by Eq. (2) with certain fitted parameters. As for the fitting parameters listed in Table I, the values of E_u and E_d are consistent with the experimental data.[15,17] However, the different values of N_{vt} have to be used for different alloy samples to get the current overall magnitude.

For hydrogenated a-Si-based alloy samples with different defect densities, the frozen-in defect densities after high-temperature annealing are found to increase with the initial defect densities $N_s(T_E)$ which are frozen-in defect densities by the usual cooling rate after deposition. The frozen-in defect densities after 400 °C FC, ΔN_s(400 °C FC), for seven alloy samples are plotted

TABLE I. Fitting parameters used for the solid curves shown in Fig. 1 with Eq. (2).

	E_u (meV)	E_d (meV)	N_{vt} ($\times 10^{20}$ cm^{-3} eV^{-1})
a-Si:H	50	0.55	2.6
a-$Si_{0.93}N_{0.07}$:H	58	0.55	3.5
a-$Si_{0.94}N_{0.06}$:H	60	0.55	4.9
a-$Si_{0.87}N_{0.13}$:H	75	0.60	9.3
a-$Si_{0.78}N_{0.22}$:H	95	0.65	8.0

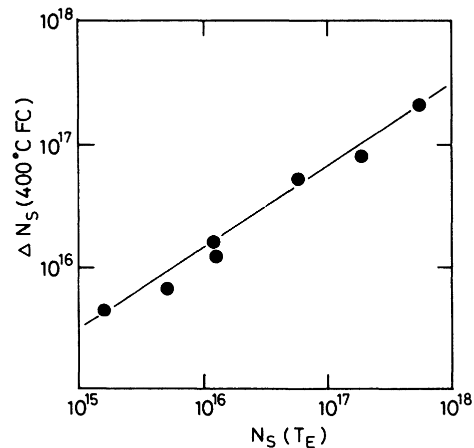

FIG. 3. Increment of the defect density after fast cooling (FC) from 400 °C versus the defect density at T_E for various alloy films.

against the $N_s(T_E)$ in Fig. 3. It is interesting that ΔN_s (400 °C FC) versus $N_s(T_E)$ shows a linear relation in logarithmic scale and the slope is about two-thirds, which means that ΔN_s(400 °C FC) follows a power-law dependence, $\Delta N_s(400\,°\mathrm{C\ FC}) \propto N_s^{2/3}(T_E)$.

B. Thickness dependence of the defect density and surface defects

There are defective layers on the free surface of *a*-Si:H and *a*-Si-based alloy films, with a density of surface defects of $(1–5)\times10^{12}$ cm^{-2}.[18] For device-quality *a*-Si:H, the bulk defect density is $(1–5)\times10^{15}$ cm^{-3}. Therefore, for a few-micrometer-thick *a*-Si:H, the number of surface defects is comparable to that of bulk defects.[17] Then in *a*-Si:H, it is meaningful to ask whether both surface and bulk defects or only bulk defects can reach thermal equilibrium. Street and Winer used *a*-Si:H with a thickness of 20–90 μm in their work to avoid the influence from surface defects. We measured the thermal-equilibrium defect density at various temperatures in *a*-Si:H and its alloy films with different thicknesses to attempt to separate the change in the density of surface defects from that of bulk ones.

Figure 4 shows the thickness dependence of the spin density in *a*-Si:H at the measurement temperatures of 200, 250, and 300 °C. The surface spin density, about 1.2×10^{12} cm^{-2}, does not exhibit an appreciable change while the bulk spin density increases from 2.3×10^{15} cm^{-3} at 200 °C to 5.1×10^{15} cm^{-3} at 300 °C. It should be pointed out that for the thinnest sample with a thickness of 0.41 μm annealing at 300 °C for 1 h resulted in some irreversible change in the spin density, which prevented us in giving a more accurate description about the behavior of surface defects in very thin films. A similar thickness dependence of defect densities was also obtained by measuring the frozen-in defects in these *a*-Si:H films. Even for the thinnest samples, the irreversible change in the defect density can be reduced within error bars illustrated in Fig. 5 because the time to hold these samples at high temperature, e.g., 350 and 400 °C, is only 10 min. If all of the data followed a set of straight lines which crossed the same intercept at zero thickness, we could say that only the bulk spins were frozen in by FC. As shown in Fig. 5, the data for two thin samples, 0.5 and 1.0 μm, deviate obviously from the straight lines, which means that the defect density in these thin samples undergoes an extra increment by FC. A relatively larger increase in

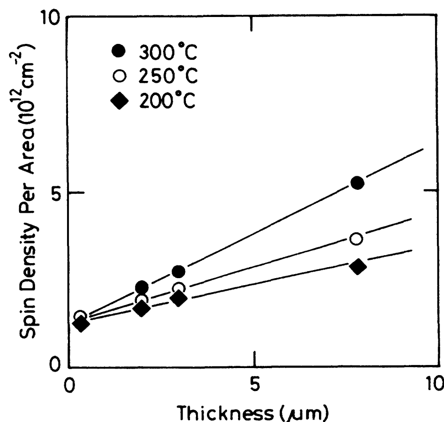

FIG. 4. Thickness dependence of the spin density in *a*-Si:H measured at 200, 250, and 300 °C.

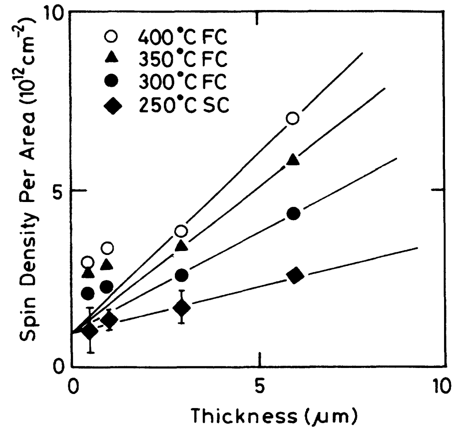

FIG. 5. Thickness dependence of the frozen-in spin density in *a*-Si:H.

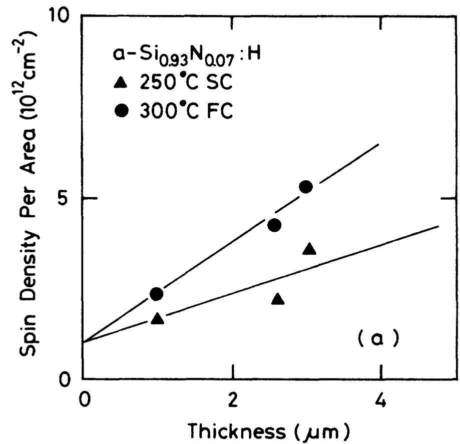

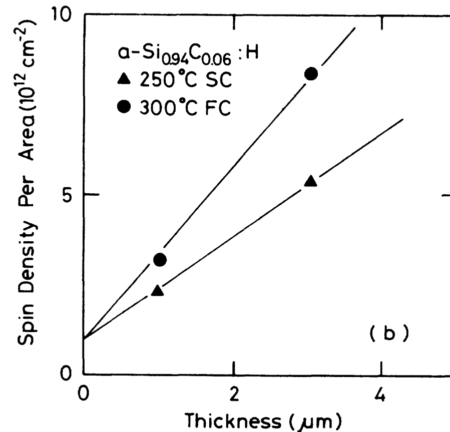

FIG. 6. Thickness dependence of spin densities both after 250 °C slow cooling (SC) and 300 °C fast cooling (FC) in (a) *a*-$Si_{0.93}N_{0.07}$:H and (b) *a*-$Si_{0.94}C_{0.06}$:H.

the spin density that appeared in thin samples cannot be simply taken as a proof that the surface defects increased with temperature; if so, all the data points should still follow the straight lines which do not verge to the same intercept at zero thickness. At the present stage, the origin of this deviation is not clear.

Thickness dependences of the spin densities for a-$Si_{0.93}N_{0.07}$:H and a-$Si_{0.94}C_{0.06}$:H alloy films both after 250 °C slow cooling (SC), and 300 °C FC are shown in Figs. 6(a) and 6(b), respectively. Although the experimental data are limited, they suggest that, for both a-$Si_{0.93}N_{0.07}$:H and a-$Si_{0.94}C_{0.06}$:H, only the bulk spin densities increased by 300 °C FC and that the surface spin densities remain unchanged around 1.0×10^{12} cm^{-2}.

Based on the previously mentioned experimental results, we can conclude that for the usual a-Si:H and its alloy films ($d>1$ μm), the surface defect density does not appreciably increase by raising temperature and the constant surface spin density (in our samples, it is about 1×10^{12} cm^{-2}) can be subtracted off to obtain the temperature dependence of the bulk defect density.

Change in the defect density is expected to affect the conductivity. From the temperature dependence of the dark conductivity, it was found that FC from the annealing temperatures above T_E reduced the dark conductivity of undoped glow-discharge (GD) a-Si:H.[4,19,20] In this work, the dark conductivity versus temperature was measured in undoped GD a-Si:H film with different thicknesses. The values of the dark conductivity above about 180 °C are independent of the thermal treatments, while below this temperature, FC reduces the dark conductivity for the thicker GD a-Si:H film (2.0 and 4.6 μm) but increases that of the thinner GD a-Si:H (0.33 μm) film. If the dark conductivity versus temperature is fitted as an exponential form in the temperature range from 150 °C to room temperature as shown in Figs. 7(a) and 7(b), the activation energy can be obtained from the experimental data. The activation energy becomes larger for the thick film and smaller for the thin film after FC, which suggests that FC makes the Fermi level shift downwards for the thick film but upwards for the thin film. The magnitude of the shift is about 0.02–0.03 eV in either case.

The relative change of the conductivity after 250 °C FC to that after 250 °C SC measured at 60 °C is shown in Fig. 8. The open symbols show the data from Ref. 20. For GD a-Si:H, with the thickness of 0.89–4.6 μm, 250 °C FC decreases the conductivity by about 20–40 %. But for 0.33-μm GD a-Si:H, 250 °C FC increases the conductivity by nearly a factor 2, this relative increase is comparable to that of sputtered (SP) a-Si:H.[20] The authors of Ref. 20

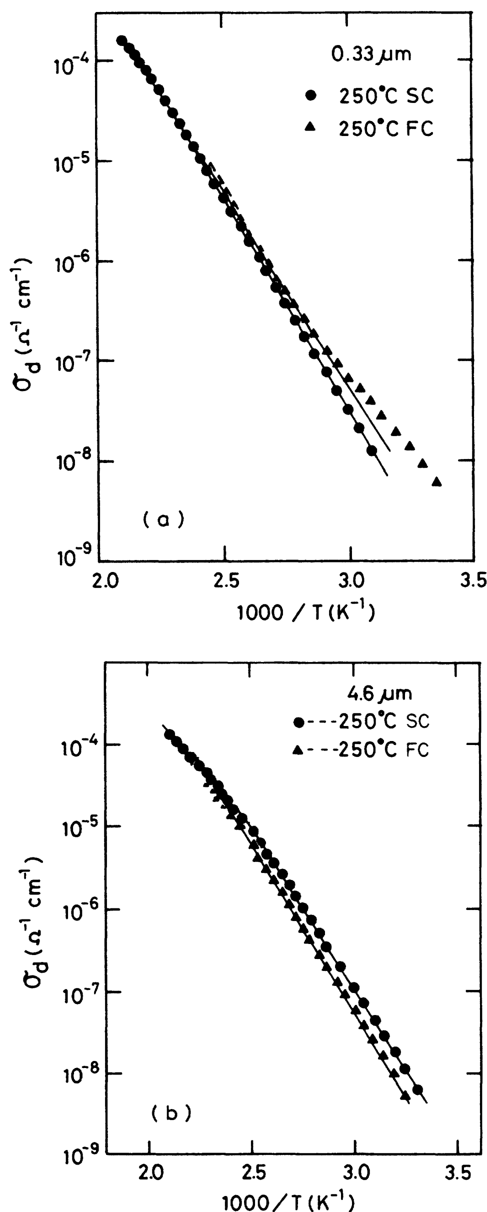

FIG. 7. Arrhenius plots of the dc conductivity σ_d in a-Si:H films with thicknesses of (a) 0.33 μm and (b) 4.6 μm after 250 °C fast cooling (FC) and 250 °C slow cooling (SC).

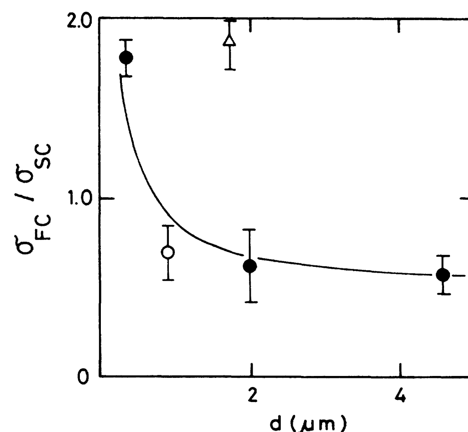

FIG. 8. Ratios of the dc conductivity after 250 °C fast cooling (FC), σ_{FC}, to that after 250 °C slow cooling (SC), σ_{SC}, measured at 60 °C vs the thickness d of a-Si:H films. Data denoted by open symbols are adopted from Ref. 20. The circles are for GD samples, and the triangle is for the sputtered sample.

attributed the difference between GD and SP a-Si:H to the poorer quality of the latter having more weak Si—Si bonds and dangling bonds.

C. Neutral and charged defects

It has been found that many charged defects exist in a-Si:H and that the incorporation of N largely increases the density of charged defects, but that of C does not change it.[15] It is interesting to see if the thermal-equilibrium process involves both neutral and charged defects, or only the neutral defects can reach thermal equilibrium in a-Si-based alloy films. For a-$Si_{0.93}N_{0.07}$:H, the ratio of the charged-bulk-defect density to the neutral one is about 8, but less than 1 for a-$Si_{0.94}C_{0.06}$:H in this work. In order to discriminate the change in the density of neutral and charged defects by FC, we carried out both CPM and LESR measurements. CPM probes both negatively charged and neutral defects mainly in bulk region, and LESR probes all charged and neutral defects.[15]

Figure 9 shows the defect densities in 3-μm-thick a-$Si_{0.93}N_{0.07}$:H, a-$Si_{0.94}C_{0.06}$:H, and a-Si:H estimated from CPM data after various thermal treatments. The defect densities are normalized to the values measured after 200 °C SC, which are 4.2×10^{16}, 5.3×10^{15}, and 4.0×10^{15} cm^{-3} for a-$Si_{0.93}N_{0.07}$:H, a-$Si_{0.94}C_{0.06}$:H, and a-Si:H, respectively. If the charged-defect density increases with temperature in a way similar to the neutral one, we should get the same temperature dependence of the defect densities both obtained by CPM and ESR. ESR measurements show that 300 °C FC increases the neutral bulk-defect density (after subtracting off the surface defects) by a factor of about 1.7 for a-$Si_{0.94}C_{0.06}$:H and 2.3 for a-$Si_{0.93}N_{0.07}$:H [see Figs. 6(a) and 6(b)], while CPM data show that 300 °C FC increases the defect density of a-$Si_{0.94}C_{0.06}$:H by a factor of 1.7, but less than 1.2 for a-$Si_{0.93}N_{0.07}$:H. The same CPM measurements were also carried out on 1-μm-thick a-Si:H, a-$Si_{0.94}C_{0.06}$:H, and a-

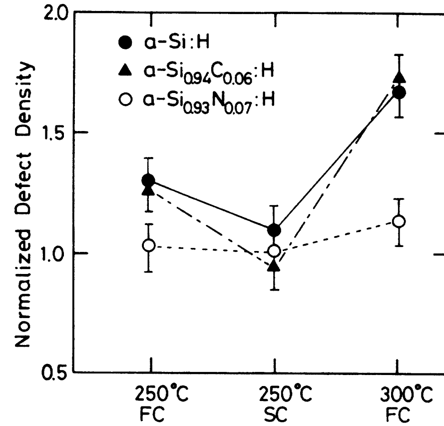

FIG. 9. Defect densities obtained by CPM after different thermal treatments.

$Si_{0.93}N_{0.07}$:H alloy films. CPM results obtained on two groups of samples with different thicknesses show that, a-$Si_{0.94}C_{0.06}$:H with a lowest fraction of charged defects has the largest relative increase, while a-$Si_{0.93}N_{0.07}$:H with a largest fraction of charged defects has the smallest relative increase in the defect density. These results imply that the frozen-in defects caused by FC are mainly contributed by neutral defects.

The data obtained by LESR measurements are listed in Table II with those by ESR and CPM. It is well known that ESR only detects the neutral dangling bond D^0, and LESR can detect both neutral and charged dangling bonds (D^+ and D^-). Then the difference in the densities of dangling bonds between LESR and ESR shows the density of the D^- and D^+. CPM is believed to be able to measure both D^0 and D^-, which should be proportional to $E+(L-E)/2$ if $N_{D^-}=N_{D^+}$ [the absolute values of the defect density calculated from CPM spectra is

TABLE II. Bulk densities of dangling bonds in a-Si:H, a-$Si_{0.94}C_{0.06}$:H, and a-$Si_{0.93}N_{0.07}$:H both after 300 °C FC and 250 °C (or 200 °C) SC derived by ESR, LESR, and CPM methods. L and E designate LESR and ESR, respectively. $g=2.0044$ and 2.010 designate the electrons and holes trapped in band tails (Ref. 19). All data are in units of 10^{16} cm^{-3}.

		ESR	LESR	$L-E$	$E+(L-E)/2$	CPM	$g=2.0044$	$g=2.010$
a-Si:H	250 °C SC	0.40	1.28	0.88	0.84	0.4	0.94	3.14
	300 °C FC	1.01	1.87	0.85	1.44	0.7	1.27	4.34
	300 °C FC / 250 °C SC	2.53	1.46	0.97	1.71	1.8	1.35	1.39
a-$Si_{1-x}C_x$:H ([C]=6 at. %)	250 °C SC	1.54	2.90	1.36	2.22	0.5	0.94	3.65
	300 °C FC	2.54	4.06	1.52	3.30	1.0	2.06	5.93
	300 °C FC / 250 °C SC	1.65	1.40	1.12	1.49	2.0	2.19	1.62
a-$Si_{1-x}N_x$:H ([N]=7 at. %)	200 °C SC	0.54	4.07	3.53	2.31	4.2	1.02	2.84
	300 °C FC	1.26	5.42	4.16	3.34	4.7	1.82	4.43
	300 °C FC / 200 °C SC	2.33	1.33	1.18	1.45	1.1	1.78	1.56

influenced by the assumptions made in the process of deducing the defect density from CPM (Ref. 20)]. Here L and E denote the bulk spin densities for LESR and ESR, respectively. A typical spectrum of the LESR for an a-$Si_{0.94}C_{0.06}$:H sample is shown in Fig. 10. The spectrum can be decomposed into three component lines with g values of 2.0055, 2.0044, and 2.010. The ESR signals with $g=2.0044$ and 2.010 for a-Si:H have been ascribed to electrons in the conduction-band tail and holes in the valence-band tail.[21] However, Morigaki suggested that these ESR signals with $g=2.0044$ and 2.010 arise from trapped electrons and holes at positively and negatively charged dangling bonds with distorted bond angles, respectively, based on the results of the optically detected magnetic-resonance measurements.[22] Wu and Stesmans also suggested that these ESR signals do not arise from the band-tail states.[23] Therefore, the origin of these signals is not clear at present. Data listed in Table II indicate that, compared with the spin densities measured after 250 °C SC, 300 °C FC increases the average density of neutral dangling bonds by a factor 2.2, but increases the charged defect density only by a factor 1.1 for three kinds of samples. As described in some details later, the frozen-in defects by FC in a-Si:H and a-$Si_{0.94}C_{0.06}$:H can be relaxed down to $1/e$ of the initial value within 10 min at 250 °C, and there is no appreciable difference observed between the spin densities measured after 250 and 200 °C SC. The results of LESR and ESR measurements also suggest that the increase in the density of neutral defects is more prominent than the increase in the density of charged defects.

LESR measurements give us another interesting result that the densities of both LESR centers with $g=2.010$ and 2.0044 increase by a factor 1.4–2.2 after 300 °C FC in a-Si:H, a-$Si_{0.93}N_{0.07}$:H, and a-$Si_{0.94}C_{0.06}$:H (see Table II). The characteristic energy of valence-band-tail E_u observed by CPM does not increase within experimental precision (±1 meV) after 300 °C FC. By light soaking, the densities of both these LESR centers do not appreciably increase although E_u slightly increases (2±1 meV).[24] Such a difference between the effect of light soaking and FC might provide some information about the origin of these two kinds of the LESR centers.

D. Relaxation behavior

For the observation of the relaxation behavior of the frozen-in defect density, the samples were first annealed at 400 °C for 10 min and rapidly cooled to room temperature for ESR measurements. The samples were then annealed at temperatures of 280, 250, 220, 200, 180, and 150 °C for a prolonged period to follow the relaxation process. Relaxation behaviors have been observed for a-Si:H, a-$Si_{1-x}C_x$:H ($x=0.06$, 0.13, and 0.20), and a-$Si_{1-x}N_x$:H ($x=0.07$, 0.11, and 0.21) alloy films. Data for a 6-μm-thick a-Si:H and a 3-μm-thick a-$Si_{0.87}C_{0.13}$:H samples are shown in Figs. 11 and 12, respectively.

As suggested by Street and Winer, the relaxation in undoped a-Si:H is nonexponential and consistent with the stretched exponential form found in doped a-Si:H.[8] The relaxation of the frozen-in defect density can be expressed as

$$\Delta N(t)=\Delta N_0 \exp[-(t/\tau)^{\beta}] , \quad (3)$$

where β is the dispersion parameter. The frozen-in defect densities in both a-$Si_{1-x}C_x$:H and a-$Si_{1-x}N_x$:H are found to follow a similar relaxation behavior to that in a-Si:H with values of β ranging from 0.4–0.6. As shown in Fig. 11, the relaxation of the frozen-in defect density in a-Si:H to $1/e$ of its initial value takes about 4×10^3 sec at 200 °C, decreasing to about 100 sec at 250 °C. These values of the relaxation time are 1 order of magnitude smaller than those reported by Street and Winer, which can be attributed to the different preparation conditions of samples.[8]

However, alloying C and N into a-Si:H films increases the relaxation time significantly. The relaxation time of

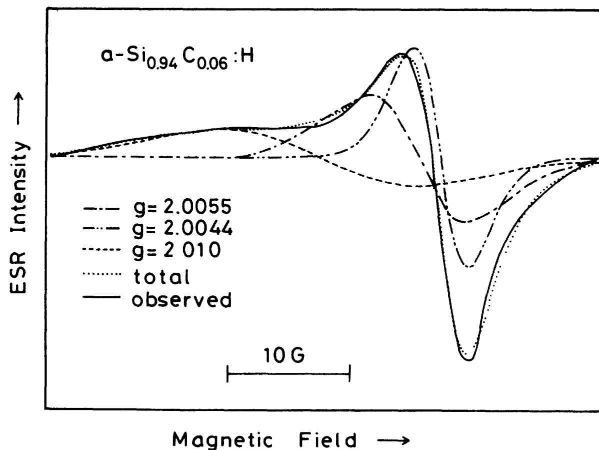

FIG. 10. An example of LESR signals at 77 K for an a-$Si_{0.87}C_{0.13}$:H sample. The observed signal (solid curve) is decomposed into three component signals with $g=2.0055$ (dash-dot curve), 2.0044 (dash-dot-dot curve), and 2.010 (dashed curve). The sum of the three component signals are shown by dotted curve.

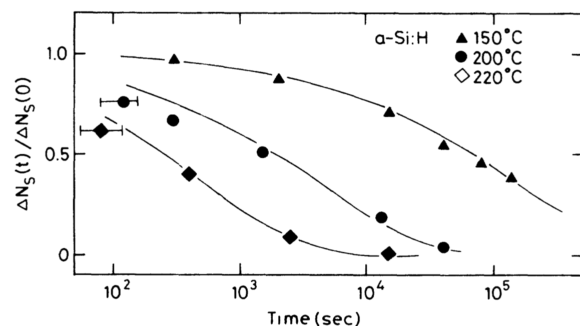

FIG. 11. Relaxation data for a 6-μm a-Si:H at 150, 200, and 250 °C after 400 °C FC. The solid curve are the fitting results with Eq. (3). Here $\Delta N_s(t)=N_s(t)-N_s(\infty)$ and $\Delta N_s(0)=N_s(0)-N_s(\infty)$. $N_s(t)$, $N_s(0)$, and $N_s(\infty)$ are the spin density at time t, the initial spin density, and the final spin density, respectively.

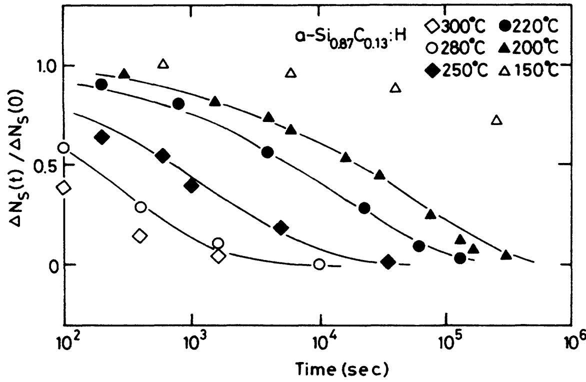

FIG. 12. Relaxation data for 3-μm a-$Si_{0.87}C_{0.13}$:H at 150, 200, 220, 250, 280, and 300 °C, respectively after 400 °C fast cooling (FC). The solid curves are the fitting results with Eq. (3). $\Delta N_s(0)$ and $\Delta N_s(t)$ are defined in the caption of Fig. 11.

a-$Si_{0.87}C_{0.13}$:H is more than 10 times larger than that of a-Si:H. At 200 °C, the relaxation time is about 4×10^4 sec for a-$Si_{0.87}C_{0.13}$:H (see Fig. 12). Solid curves in Figs. 11 and 12 are theoretically calculated results using Eq. (3) with relaxation time τ and dispersion parameter β as the fitting parameters. The stretched exponential relaxation has been interpreted in terms of the dispersive diffusion of hydrogen in the exponential distribution of trapping sites. The dispersion parameter β is given by $\beta=T/T_0$, where T_0 is the characteristic temperature of the exponential distribution of trapping sites and T is the measurement temperature.[25] The values of β obtained from the fitting curves in Fig. 12 for a-$Si_{0.87}C_{0.13}$:H increases slightly with the temperature, from 0.50±0.02 at 200 °C to 0.60±0.02 at 280 °C, which is consistent with the relation $\beta=T/T_0$ if we take T_0 to be 870 K for a-$Si_{0.87}C_{0.13}$:H. But for a-Si:H, the values of T_0 obtained from Fig. 11 is about 900 K. According to the proposition of Street and Winer that the distribution of hydrogen bonding energies should be closely related to that of the defect-formation energies, T_0 should be equal to $2T_V$, where kT_V is the characteristic energy of valence-band-tail states.[8] The magnitudes of T_0 estimated from our experimental data are between T_V and $2T_V$, i.e., $T_V < T_0 < 2T_V$.

For both doped and undoped a-Si:H, the relaxation time τ has been found to be thermally activated,

$$\tau(T)=\tau_0\exp(E_B/kT)\ , \tag{4}$$

where E_B is the energy barrier for structural rearrangement. Here we extend this equation to our undoped hydrogenated a-Si-based alloys. The relaxation time τ is plotted against the temperature for three different alloy samples in Fig. 13, in which the data of a-Si:H are also shown for comparison. The different magnitude of the relaxation time at the certain temperature should result from both the change in prefactor τ_0 and the energy barrier E_B or either. If the temperature-dependent relaxation time is fitted to Eq. (4) with the same value of the prefactor and different values of E_B for these alloys, the

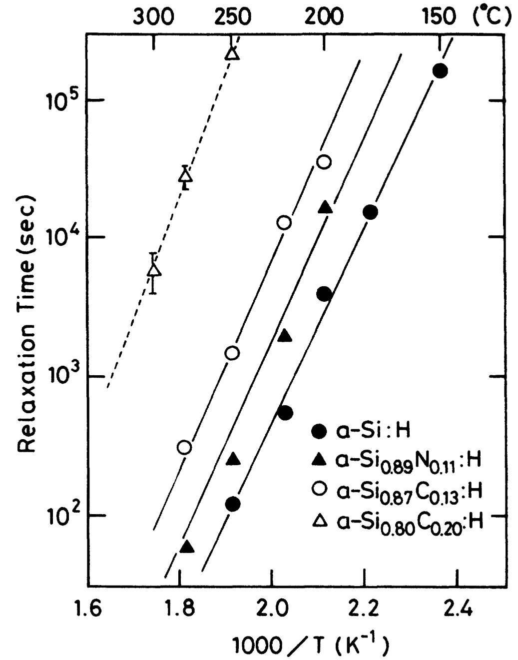

FIG. 13. Temperature dependence of the relaxation time for a-Si:H and its alloy films.

values of E_B are 1.54, 1.50, and 1.45 eV for a-$Si_{0.87}C_{0.13}$:H, a-$Si_{0.89}N_{0.11}$:H, and a-Si:H, respectively. Because of the limited experimental data for a-$Si_{0.80}C_{0.20}$:H, only the roughly estimated value can be obtained to be between 1.55 and 1.70 eV.

Figure 13 also provides some information about "thermal-equilibrium temperature" T_E. If we define T_E

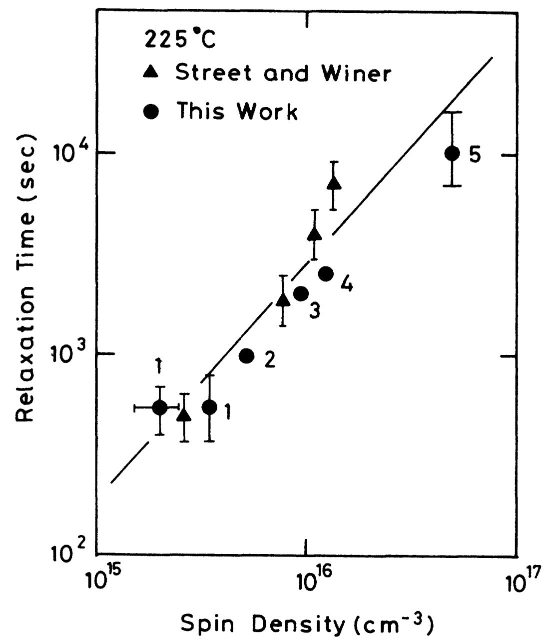

FIG. 14. Relaxation time vs the spin density in a-Si:H and its alloy films. The triangles for a-Si:H are adopted from Ref. 8. The numbers 1, 2, 3, 4, and 5 designate a-Si:H, a-$Si_{0.93}N_{0.07}$:H, a-$Si_{0.89}N_{0.11}$:H, a-$Si_{0.94}C_{0.06}$:H, and a-$Si_{0.87}C_{0.13}$:H, respectively.

to be the temperature at which $\tau(T_E)=10$ min, the T_E's are about 220, 240, and 260 °C for a-Si:H, a-$Si_{0.89}N_{0.11}$:H, and a-$Si_{0.87}C_{0.13}$:, respectively, values which are comparable to those of $T_E(20\%)$ that we reported before for a-Si:H, a-$Si_{0.95}C_{0.05}$:H, and a-$Si_{0.82}C_{0.18}$:H (some difference may be due to the insufficient annealing in previous cases when we did not know the relaxation time for these alloy films).[5] $T_E(20\%)$ denotes the temperature from which FC increases the spin densities by 20% compared with those after SC. By the extrapolation of the limited experimental data in Fig. 13, we can estimate T_E for a-$Si_{0.80}C_{0.20}$:H to be around 320 °C. These T_E's are shown in Fig. 1 by arrows.

Dependence of the relaxation time at 225 °C on the spin density is shown in Fig. 14 including the data adopted from Ref. 8. It is noteworthy that the relaxation time increases with an increase in the spin density caused by alloying C or N, which is similar to the increase in the relaxation time with an increase in the spin density in a-Si:H.[8] As predicted by H-glass model,[8] the sample with the highest defect density should have the longest relaxation time because a larger defect density should be associated with a broader distribution of H bonding energies.

IV. CONCLUSION

Temperature dependences of the defect densities in hydrogenated a-Si-based alloy films obtained both by ESR measurements of frozen-in defects after FC and *in situ* ESR measurements at elevated temperatures agree quite well with each other, which suggests that the frozen-in defect density is the thermal-equilibrium defect density at the annealing temperature.

Frozen-in defect densities in these alloys increase with defect density at T_E, following a two-thirds power law of $N_{S(T_E)}$.

The surface defects do not appear to be involved in the thermal-equilibrium process in thick films (> 1 μm). But extra defect creation by FC in addition to thermal equilibrium defects were observed for the films thinner than 1 μm.

The charged-defect density in these alloy films does not increase appreciably by FC. However, both the LESR centers with $g=2.0044$ and $g=2.010$ increase prominently by FC, while light soaking does not appreciably change them.

Relaxation behavior of frozen-in defect density in the alloys also follow the stretched exponential form as that in a-Si:H. The magnitudes of dispersion parameter β estimated from experimental results are between $T/2T_V$ and T/T_V.

ACKNOWLEDGMENTS

The authors are grateful to H. Kidoh, M. Sasaki, T. Oh-hashi, N. Awaki, and H. Asada for their help with the experiments. This work was partially supported by the Sunshine Project of the Ministry of International Trade and Industry of Japan.

*On leave from Department of Physics, Lanzhou University, Lanzhou, Gansu, China.

[1] Z. E. Smith and S. Wagner, Phys. Rev. B **32**, 5510 (1985).

[2] Z. E. Smith, S. Aljishi, D. Slobodin, V. Chu, S. Wagner, P. M. Lenahan, R. R. Arya, and M. S. Bennett, Phys. Rev. Lett. **57**, 2450 (1986).

[3] T. J. McMahon and R. Tsu, Appl. Phys. Lett. **51**, 412 (1987).

[4] X. Xu, A. Morimoto, M. Kumeda, and T. Shimizu, Appl. Phys. Lett. **52**, 622 (1988).

[5] X. Xu, A. Okumura, A. Morimoto, M. Kumeda, and T. Shimizu, Phys. Rev. B **38**, 8371 (1988).

[6] X. Xu, A. Morimoto, M. Kumeda, and T. Shimizu, in Vol. 149 of *Materials Research Society Symposium Proceedings*, edited by Y. Hamakawa, P. G. LeComber, A. Madan, P. C. Taylor, and M. J. Thompson (Materials Research Society, Pittsburgh, 1989), p. 143.

[7] S. Zafar and E. A. Schiff, J. Non-Cryst. Solids **114**, 618 (1989).

[8] R. A. Street and K. Winer, Phys. Rev. B **40**, 6236 (1989).

[9] Z. E. Smith and S. Wagner, Phys. Rev. Lett. **59**, 688 (1987).

[10] Z. E. Smith and S. Wagner, in *Amorphous Silicon and Related Materials*, edited by H. Fritzche (World Scientific, Singapore, 1989), p. 409.

[11] Y. Bar-Yam, D. Adler, Phys. Rev. Lett. **51**, 467 (1986).

[12] G. Muller, S. Kalbitzer, and H. Mannsperger, Appl. Phys. A **39**, 243 (1986).

[13] S. Zafar and E. A. Schiff, Phys. Rev. B **40**, 5235 (1989).

[14] J. Z. Liu, V. Chu, D. S. Shen, D. Slobodin, and S. Wagner, Phys. Rev. B **40**, 6424 (1989).

[15] T. Shimizu, H. Kidoh, A. Morimoto, M. Kumeda, Jpn. J. Appl. Phys. **28**, 586 (1989).

[16] M. Vaněček, J. Kočka, J. Stuchlík, O. Stika, and Tříska, Sol. Energy Mater. **8**, 411 (1983).

[17] J. Bullot and M. P. Schmidt, Phys. Status Solidi B **143**, 345 (1987).

[18] T. Shimizu, X. Xu, H. Kidoh, A. Morimoto, and M. Kumeda, J. Appl. Phys. **64**, 5045 (1988).

[19] E. Smith, S. Aljishi, D. S. Shen, V. Chu, D. Slobodin, and S. Wagner, in *Stability of Amorphous Silicon Alloy Materials and Devices*, Proceedings of an International Conference on Stability of Amorphous Silicon Alloy Materials and Devices, AIP Conf. Proc. No. 157, edited by B. L. Stafford and E. Sabinsky (AIP, New York, 1987).

[20] R. Meaudre, P. Jensen, and M. Meaudre, Phys. Rev. B **38**, 12 449 (1988).

[21] R. A. Street and D. K. Biegelsen, Solid State Commun. **33**, 1159 (1980).

[22] K. Morigaki, J. Non-Cryst. Solids **77/78**, 583 (1985).

[23] Y. Wu and A. Stesmans, Phys. Rev. B **38**, 2779 (1988).

[24] T. Shimizu, H. Kidoh, M. Matsumoto, A. Morimoto, and M. Kumeda, J. Non-Cryst. Solids **114**, 630 (1989).

[25] J. Kakalios, R. A. Street, and W. B. Jackson, Phys. Rev. Lett. **59**, 1037 (1987).